Continuous phase transition between Néel and valence bond solid phases in a J-Q-like spin ladder system

Takuhiro Ogino,[1] Ryui Kaneko,[2,1] Satoshi Morita,[1] Shunsuke Furukawa,[3] and Naoki Kawashima[1]
[1]*Institute for Solid State Physics, University of Tokyo, Kashiwa, Chiba 277-8581, Japan*
[2]*Department of Physics, Kindai University, Higashi-Osaka, Osaka 577-8502, Japan*
[3]*Department of Physics, Keio University, Kohoku-ku, Yokohama, Kanagawa 223-8522, Japan*

(Received 26 October 2020; revised 19 January 2021; accepted 25 January 2021; published 11 February 2021)

We investigate a quantum phase transition between a Néel phase and a valence bond solid (VBS) phase, each of which breaks a different $\mathbb{Z}_2$ symmetry, in a spin-1/2 two-leg XXZ ladder with a four-spin interaction. The model can be viewed as a one-dimensional variant of the celebrated J-Q model on a square lattice. By means of variational uniform matrix product state calculations and an effective field theory, we determine the phase diagram of the model and present evidence that the Néel-VBS transition is continuous and belongs to the Gaussian universality class with the central charge $c = 1$. In particular, the critical exponents β, η, and, ν are found to satisfy the constraints expected for a Gaussian transition within numerical accuracy. These exponents do not detectably change along the phase boundary while they are in general allowed to do so for the Gaussian class.

DOI: 10.1103/PhysRevB.103.085117

I. INTRODUCTION

Continuous transitions do not occur between two phases in which different symmetries are broken spontaneously, according to the Landau-Ginzburg-Wilson paradigm. Contrary to this conventional wisdom, Senthil *et al.* proposed a deconfined quantum critical point (DQCP) at which a direct continuous transition between a Néel phase and a valence bond solid (VBS) phase occurs in a two-dimensional (2D) spin-1/2 system [1,2]. The 2D DQCP is characterized by deconfined spin-1/2 spinons coupled to an emergent U(1) gauge field, which results in the same critical exponents for the order parameters in the Néel and VBS phases. An unusually large anomalous dimension η is also expected because the spinons coupled to the emergent gauge field are not at all free particles.

One of the simplest microscopic models that may realize deconfined quantum criticality (DQC) is the J-Q model on a 2D square lattice [3]. The model consists of the nearest-neighbor Heisenberg interaction J and a four-spin interaction Q, and exhibits a phase transition between a Néel phase and a VBS phase. A quantum Monte Carlo (QMC) study suggests a continuous nature of the Néel-VBS transition, nearly the same critical exponents for the magnetic and VBS order parameters, the unusually large anomalous dimension $\eta = 0.26 \pm 0.03$, and the emergent U(1) symmetry, consistent with DQC scenario [1,2]. On the other hand, the possibility of a weak first-order transition, where the correlation length would exceed an accessible system size, cannot be ruled out [4,5]. Later, larger systems and higher symmetry [SU(N) with $N = 2, 3, 4$] were explored [6], which revealed unusually strong corrections to scaling that make the estimate of critical indices systematically drift even beyond $L = 256$, while the finite-size-scaling plot seemed reasonably good for restricted size windows. These observations clearly show computational difficulty in diagnosing a DQC in two spatial dimensions.

Recently, DQC in one spatial dimension has been intensively studied [7–14]. This is because analytical approaches such as bosonization and a slave particle theory may help understand the nature of DQC, especially in one dimension. In addition, numerical methods based on matrix product states (MPSs) are applicable to a rich variety of models, including frustrated ones in one dimension. We note that a continuous symmetry breaking is prohibited in 1D quantum systems unless the uniform magnetic susceptibility diverges [15]. Therefore, we have to introduce, for example, easy-axis anisotropy or long-range exchange interactions to realize a magnetic long-range order. The former examples include an anisotropic XZ model with nearest- and next-nearest-neighbor interactions [7,8]. The model has a ferromagnetic (FM) phase and a VBS phase, each of which breaks a different $\mathbb{Z}_2$ symmetry. The transition between the two phases was found to be continuous and to be characterized by the central charge $c = 1$. The critical exponents in the FM phase are very close to those in the VBS phase and change continuously along the phase boundary. The latter examples include the J-Q chain with long-range Heisenberg interactions [16]. The model exhibits an AFM-VBS transition, which takes place between two gapless phases.

In this paper, we investigate a quantum phase transition between two ordered phases, in which different $\mathbb{Z}_2$ symmetries are broken, in a J-Q-like model on a two-leg ladder. In contrast to the FM-VBS transition studied in Refs. [7,8], we propose a model which realizes a Néel phase and the VBS phase, as the original 2D J-Q model does. Our model consists of short-range interactions up to four neighboring sites. We introduce easy-axis XXZ anisotropy to realize the Néel phase.

The four-spin interaction Q on each plaquette of a square lattice reduces to that on each plaquette of a two-leg ladder. For simplicity, we omit the four-spin interaction between rungs and keep only that between the legs, which we call J_4. The J_4 interaction introduces effective repulsion between singlet pairs on each plaquette and induces a staggered dimer (SD) phase, which is a type of VBS phase. Analyzing this model will provide a step toward understanding the relationship between the Néel-VBS transitions in one dimension [9,17–22] and those in two dimensions [1–3].

We obtain the ground-state phase diagram of the spin-1/2 XXZ model on a two-leg ladder with the four-spin interaction by means of numerical calculations and an effective field theory. We obtain a rung singlet (RS) phase, the Néel phase, and the SD phase as the four-spin interaction J_4 is increased. The effective field theory for weak interchain couplings, which is based on bosonization, suggests that the RS-Néel transition belongs to the $(1+1)$-dimensional Ising universality class and the Néel-SD transition belongs to the Gaussian universality class. However, this observation is based on leading terms in the effective Hamiltonian and it is not obvious whether possible perturbations can modify the scenario. Furthermore, the effective field theory may fail when the interchain couplings are comparable to the intrachain coupling. For these reasons, we numerically study the Néel-SD transition. Our numerical calculations are based on the variational uniform matrix product state algorithm (VUMPS) [23,24], by which the ground state of the translationally invariant infinite system can be obtained in the form of an MPS. Our numerical results support the scenario that the Néel-SD (VBS) transition in the 1D J-Q-like model belongs to the Gaussian universality class.

We comment on an important difference between our model and the original J-Q model studied in Ref. [3]: the four-spin interaction has the positive coefficient $J_4 > 0$ in the former and the negative coefficient $-Q < 0$ in the latter. Therefore, the original J-Q model exhibits a columnar dimer (CD) phase instead of the SD phase. With a positive coefficient $-Q > 0$, the J-Q model on a square lattice is also expected to exhibit the SD phase, which has indeed been found in a closely related model with ring exchange [25]. However, detailed properties of the Néel-SD transition have yet to be explored on a square lattice because the QMC suffers from a sign problem for $-Q > 0$ (see Refs. [26–28] for related studies on the Néel-SD transition in two dimensions). In contrast, with a negative coefficient $J_4 < 0$, our model on a ladder exhibits a transition between the RS and CD phases, and the Néel phase does not appear between them (this can be understood from the field-theoretical analysis in Sec. III). This suggests that the models with a positive coefficient in the four-spin interaction are more suitable for studying the relationship between the Néel-VBS transitions in one and two dimensions. This observation, together with indications of the continuous Néel-SD (VBS) transition on a ladder in the present study, would stimulate a numerical study on the J-Q model with $-Q > 0$ on a square lattice using, e.g., tensor network algorithms [29–31].

We organize this paper as follows. In Sec. II, we introduce our model and briefly review the previous related studies. In Sec. III, we present a field-theoretical analysis for weak interchain couplings. In Sec. IV, we present a detailed numerical analysis on the transition between the Néel phase and the VBS (SD) phase. In Sec. V, we draw our conclusion.

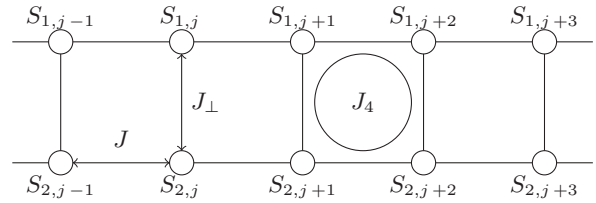

FIG. 1. Two-leg XXZ spin ladder system with a four-spin interaction, which is described by the Hamiltonian in Eq. (1).

II. MODEL

We study a spin-1/2 ladder model which is described by the Hamiltonian

$$H := J\sum_{\alpha=1,2}\sum_j (\boldsymbol{S}_{\alpha,j}\cdot\boldsymbol{S}_{\alpha,j+1})_\Delta + J_\perp\sum_j (\boldsymbol{S}_{1,j}\cdot\boldsymbol{S}_{2,j})_\Delta + J_4\sum_j (\boldsymbol{S}_{1,j}\cdot\boldsymbol{S}_{1,j+1})(\boldsymbol{S}_{2,j}\cdot\boldsymbol{S}_{2,j+1}), \tag{1}$$

with

$$(\boldsymbol{S}_{\alpha,i}\cdot\boldsymbol{S}_{\beta,j})_\Delta := S^x_{\alpha,i}S^x_{\beta,j} + S^y_{\alpha,i}S^y_{\beta,j} + \Delta S^z_{\alpha,i}S^z_{\beta,j}. \tag{2}$$

Here, the J and $J_\perp$ terms represent the nearest-neighbor XXZ interactions with the anisotropy parameter Δ along the legs and the rungs, respectively, and the J_4 term represents the four-spin interactions (Fig. 1). Throughout this paper, we take the leg interaction $J = 1$ as the unit of energy and focus on the case of $J_\perp, J_4 \geqslant 0$ and Δ close to unity.

When $J_4 = 0$ and $\Delta = 1$, the model in Eq. (1) is a standard antiferromagnetic Heisenberg model on a ladder. For $J_\perp > 0$, it shows an RS phase [Fig. 2(a)] [32–34], which has a unique ground state below an excitation gap. The case in which the anisotropy Δ is introduced for the leg interaction has also been investigated by field-theoretical and numerical approaches [32,33,35]. In the proposed phase diagram, the Néel phase with an antiferromagnetic order along the z axis [Fig. 2(c)] appears for easy-axis anisotropy $\Delta > 1$ and the sufficiently weak antiferromagnetic interchain coupling $J_\perp > 0$. The Néel phase has two degenerate ground states below an excitation gap and is characterized by the order parameter

$$\langle\mathcal{O}_{\text{Néel}}(j)\rangle = \tfrac{1}{4}\langle S^z_{1,j} - S^z_{2,j} - S^z_{1,j+1} + S^z_{2,j+1}\rangle. \tag{3}$$

In this phase, a $\mathbb{Z}_2$ symmetry with respect to the global π rotation of spins about the x axis ($S^y_{\alpha,j} \mapsto -S^y_{\alpha,j}$ and $S^z_{\alpha,j} \mapsto -S^z_{\alpha,j}$) is spontaneously broken.

The case of $J_\perp = 0$ and $\Delta = 1$ has been studied as a 1D spin-orbital model. At $J_4 = 4$, the model has an enhanced SU(4) symmetry and is solvable by the Bethe ansatz [36]. At this point, the system is gapless and is described effectively by the $\text{SU}(4)_1$ Wess-Zumino-Witten (WZW) model with the central charge $c = 3$ [37,38]. Through numerical and field-theoretical analyses [39,40], it has been found that a gapless phase continues for $J_4 \geqslant 4$ while a SD phase [Fig. 2(b)] with two degenerate ground states below an excitation gap appears for $0 < J_4 < 4$. The SD phase is characterized by the order

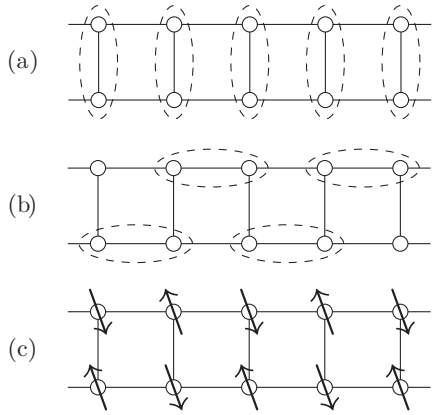

FIG. 2. (a) The rung singlet (RS) phase, (b) the staggered dimer (SD) phase, and (c) the Néel phase. Two spins enclosed by a dashed line form a singlet. The SD phase spontaneously breaks a $\mathbb{Z}_2$ symmetry with respect to the rung-centered reflection. The Néel phase has an antiferromagnetic order along the z axis and spontaneously breaks a $\mathbb{Z}_2$ symmetry with respect to the global π rotation of spins about the x axis. In this phase, the ordered moment $\langle S^z_{\alpha,i}\rangle$ shows a staggered pattern along both the leg and rung directions.

parameter

$$\langle \mathcal{O}_{\rm SD}(j)\rangle = \tfrac{1}{4}\langle \boldsymbol{S}_{1,j-1}\cdot\boldsymbol{S}_{1,j} - \boldsymbol{S}_{2,j-1}\cdot\boldsymbol{S}_{2,j} - \boldsymbol{S}_{1,j}\cdot\boldsymbol{S}_{1,j+1} + \boldsymbol{S}_{2,j}\cdot\boldsymbol{S}_{2,j+1}\rangle. \quad (4)$$

In this phase, a $\mathbb{Z}_2$ symmetry with respect to the rung-centered reflection ($\boldsymbol{S}_{\alpha,j} \mapsto \boldsymbol{S}_{\alpha,-j}$) is spontaneously broken. Intuitively, the SD order is a consequence of effective repulsion between singlet pairs in the same plaquette due to J_4.

When both $J_\perp > 0$ and $J_4 > 0$ are present in the isotropic case $\Delta = 1$, the RS and SD phases compete. The boundary between these phases in the $J_\perp$-J_4 plane has been obtained numerically for $0 < J_\perp, J_4 \lesssim 2$ [41,42]. Field-theoretical analyses for weak interchain couplings [42–45] suggest that this transition is continuous and is described by the $SU(2)_2$ WZW theory (equivalent to three copies of free massless Majorana fields) with the central charge $c = 3/2$. The exact diagonalization result of Ref. [41] is consistent with this scenario for $0.5 \lesssim J_\perp \lesssim 1.5$. We note that the phase diagram is expected to have a more complex structure for larger J_4. In fact, for $J_4 = 4$, the exact solution of Ref. [36] can be extended for $J_\perp \neq 0$ [46]. It shows two gapless phases over $J_\perp < -\pi/2\sqrt{3} + (\ln 3)/2 (\simeq -0.36)$ and $-\pi/2\sqrt{3} + (\ln 3)/2 < J_\perp < 4$ as well as the gapped RS phase for $J_\perp > 4$.

In this paper, we consider the case in which Δ is slightly larger than unity, i.e., in a weakly easy-axis regime. We find that there appears a finite region of the Néel phase that intervenes between the RS and SD phases (see Fig. 3 presented later). This Néel phase is expected to be adiabatically connected to the one discussed for the XXZ ladder in Refs. [32,33,35]. It is remarkable that just the addition of small Ising interactions ($\Delta - 1 > 0$) changes the phase structure. This phase structure can be derived in the field-theoretical analysis for weak interchain couplings $0 \leqslant J_\perp, J_4 \ll 1$ (Sec. III) and is numerically confirmed for $J_\perp = 1$ (Sec. IV). Our particular interest lies in the nature of the transition between the Néel and SD phases, each of which spontaneously breaks a different $\mathbb{Z}_2$ symmetry.

In passing, we note that our model in Eq. (1) has a close relationship with a spin-1/2 Heisenberg ladder with a ring exchange studied in Refs. [47–50]. The ring exchange interaction is derived from the fourth-order perturbation theory of the Hubbard model and its effects have been discussed for the ladder compound $La_6Ca_8Cu_{24}O_{41}$ [51,52]. On each plaquette of the ladder, this interaction appears in the form

$$\begin{aligned}&\boldsymbol{S}_{1,j}\cdot\boldsymbol{S}_{2,j} + \boldsymbol{S}_{1,j+1}\cdot\boldsymbol{S}_{2,j+1} + \boldsymbol{S}_{1,j}\cdot\boldsymbol{S}_{1,j+1}\\ &+ \boldsymbol{S}_{2,j}\cdot\boldsymbol{S}_{2,j+1} + \boldsymbol{S}_{1,j}\cdot\boldsymbol{S}_{2,j+1} + \boldsymbol{S}_{2,j}\cdot\boldsymbol{S}_{1,j+1}\\ &+ 4(\boldsymbol{S}_{1,j}\cdot\boldsymbol{S}_{2,j})(\boldsymbol{S}_{1,j+1}\cdot\boldsymbol{S}_{2,j+1})\\ &+ 4(\boldsymbol{S}_{1,j}\cdot\boldsymbol{S}_{1,j+1})(\boldsymbol{S}_{2,j}\cdot\boldsymbol{S}_{2,j+1})\\ &- 4(\boldsymbol{S}_{1,j}\cdot\boldsymbol{S}_{2,j+1})(\boldsymbol{S}_{2,j}\cdot\boldsymbol{S}_{1,j+1}). \quad (5)\end{aligned}$$

The Heisenberg ladder with a ring exchange has been found to show a transition between the RS and SD phases [47–50], similar to the model in Eq. (1) with $\Delta = 1$. Therefore, the two models are expected to share similar phase structures in the presence of XXZ anisotropy. Our motivation to focus on the simplified four-spin interaction $(\boldsymbol{S}_{1,j}\cdot\boldsymbol{S}_{1,j+1})(\boldsymbol{S}_{2,j}\cdot\boldsymbol{S}_{2,j+1})$ instead of the ring exchange in Eq. (5) lies in a connection with the 2D J-Q model and simplicity in applying bosonization.

III. EFFECTIVE FIELD THEORY FOR WEAK INTER-CHAIN COUPLINGS

A. Bosonization

For weak interchain couplings with $|J_\perp|, |J_4| \ll 1$, the ground-state phase diagram of the model in Eq. (1) can be studied by means of effective field theory based on bosonization [53,54]. Our formulation is an extension of those in Refs. [32–34,42,43,45] and we take similar notations as those in Ref. [45]. Our starting point is the two decoupled XXZ chains obtained for $J_\perp = J_4 = 0$. In this case, each chain labeled by $\alpha = 1, 2$ is described effectively by the quantum sine-Gordon Hamiltonian:

$$H^{\rm eff}_\alpha = \int {\rm d}x \frac{v}{2}[K^{-1}(\partial_x\phi_\alpha)^2 + K(\partial_x\theta_\alpha)^2] - \frac{v\lambda}{2\pi}\cos(4\sqrt{\pi}\phi_\alpha). \quad (6)$$

Here, the bosonic field $\phi_\alpha(x)$ and its dual counterpart $\theta_\alpha(x)$ satisfy the commutation relation $[\phi_\alpha(x), \theta_\beta(x')] = -i\delta_{\alpha\beta}\vartheta_{\rm step}(x - x')$, with $\vartheta_{\rm step}(\cdot)$ being the Heaviside step function. For $\Delta \leqslant 1$, the λ term is irrelevant (marginally irrelevant at $\Delta = 1$) and thus the effective Hamiltonian in the infrared limit is given by the Gaussian part of Eq. (6), which is known as the Tomonaga-Luttinger liquid (TLL) theory. In this limit, the spin velocity v and the TLL parameter K can be obtained exactly from the Bethe ansatz. The TLL parameter K monotonically decreases as a function of Δ and reaches $K = 1/2$ at $\Delta = 1$. When Δ exceeds unity, the λ term with the scaling dimension $4K$ becomes relevant (i.e., $4K < 2$) and grows along the renormalization group (RG) flow. Owing to $\lambda > 0$, this term eventually leads to the locking of the bosonic

field at $2\sqrt{\pi}\phi_\alpha = 0, \pi$, which correspond to the Néel order in the z direction [as seen in Eq. (7a) below]. In this case, K and λ depend on the scale of our concern. We note that for $\Delta > 1$ and with an infinitesimal antiferromagnetic interchain coupling $J_\perp > 0$, the Néel states on the individual chains are interlocked, leading to the Néel state on a ladder [Fig. 2(c)] as discussed in Refs. [32,33,35].

The spin operators on each chain are related to the bosonic fields as

$$S^z_{\alpha,j} = \frac{a}{\sqrt{\pi}}\partial_x\phi_\alpha + (-1)^j a_1 \cos(2\sqrt{\pi}\phi_\alpha) + \cdots, \quad (7a)$$

$$S^+_{\alpha,j} = e^{i\sqrt{\pi}\theta_\alpha}[b_0(-1)^j + b_1\cos(2\sqrt{\pi}\phi_\alpha) + \cdots], \quad (7b)$$

where the fields are taken at $x = ja$ with a being the lattice constant. Furthermore, the dimer operators, i.e., the product of neighboring spins, are also related to the fields as

$$S^z_{\alpha,j}S^z_{\alpha,j+1} = (-1)^j d_z \sin(2\sqrt{\pi}\phi_\alpha) + \cdots, \quad (8a)$$

$$S^x_{\alpha,j}S^x_{\alpha,j+1} + S^y_{\alpha,j}S^y_{\alpha,j+1} = (-1)^j d_{xy}\sin(2\sqrt{\pi}\phi_\alpha) + \cdots, \quad (8b)$$

where the fields are taken at $x = (j+1/2)a$ and the uniform component is omitted for simplicity. The nonuniversal coefficients a_1, b_0, b_1, d_z, and d_{xy} in Eqs. (7) and (8) have been determined analytically and numerically for $\Delta < 1$ [45,55–57]. For $\Delta = 1$, these coefficients depend on the scale of our concern because of the presence of the marginally irrelevant perturbation; at a fixed length scale, they should satisfy $a_1 = b_0 =: \bar{a}$ and $d_z = d_{xy}/2 =: \bar{d}$ because of the SU(2) symmetry.

Let us now include the interchain couplings, $J_\perp$ and J_4, perturbatively. Using Eqs. (7) and (8) for the interchain couplings, the low-energy effective Hamiltonian of Eq. (1) is obtained as

$$\begin{aligned} H^{\rm eff} = \int {\rm d}x \sum_{q=\pm} \frac{v_q}{2}\left[K_q^{-1}(\partial_x\phi_q)^2 + K_q(\partial_x\theta_q)^2\right] \\ + g_+\cos(2\sqrt{2\pi}\phi_+) + g_-\cos(2\sqrt{2\pi}\phi_-) \\ + \tilde{g}_-\cos(\sqrt{2\pi}\theta_-) + \cdots. \end{aligned} \quad (9)$$

Here, we introduced symmetric and antisymmetric combinations of the fields, $\phi_\pm := (\phi_1 \pm \phi_2)/\sqrt{2}$ and $\theta_\pm := (\theta_1 \pm \theta_2)/\sqrt{2}$. The coupling constants in Eq. (9) are given in terms of the interchain couplings as

$$g_\pm = \frac{1}{a}\left(J_\perp\Delta\frac{a_1^2}{2} \mp J_4\frac{(3d)^2}{2}\right), \quad \tilde{g}_- = \frac{1}{a}J_\perp b_0^2, \quad (10)$$

where $3d := d_{xy} + d_z$. Furthermore, the velocities $v_\pm$ and the TLL parameters $K_\pm$ are now defined for the symmetric and antisymmetric channels and they are in general modified from the values v and K in the decoupled XXZ chains by the effects of the interchain couplings. In Eq. (9), we focused on terms that are most important around the SU(2)-symmetric case $\Delta = 1$. Indeed, the $g_\pm$ and $\tilde{g}_-$ terms have the scaling dimensions $2K_\pm$ and $1/(2K_-)$, respectively, which are all equal to unity in the limit of the decoupled Heisenberg chains. These terms are much more relevant, in the RG sense, than the λ term with the scaling dimension $2K_+ + 2K_-$ in Eq. (6). Therefore, the λ term can be ignored unless the anisotropy $\Delta - 1$ is significantly larger than $J_\perp$ and J_4.

B. Expected phase diagram

The effective Hamiltonian in Eq. (9) indicates a separation of the symmetric and antisymmetric channels. The symmetric channel is described by the sine-Gordon model, in which the strongly relevant g_+ term leads to the locking of ϕ_+ at distinct positions depending on the sign of g_+. A Gaussian-type transition with the central charge $c = 1$ is expected at $g_+ = 0$. The antisymmetric channel is described by the dual-field double sine-Gordon model, in which the strongly relevant g_- and $\tilde{g}_-$ terms compete. When $K_- = 1/2$, both terms have the same scaling dimensions of unity, and the long-distance physics can be determined by simply examining which of $|g_-|$ and $|\tilde{g}_-|$ is larger (in this case, the model is known as the self-dual sine-Gordon model [58]). Namely, $|g_-| > |\tilde{g}_-|$ ($|g_-| < |\tilde{g}_-|$) leads to the locking of ϕ_- (θ_-). In fact, the self-dual sine-Gordon model can be mapped onto two free Majorana fields—one of them is always massive (unless $g_- = \tilde{g}_- = 0$) while the other is massless at $|g_-| = |\tilde{g}_-|$ and massive otherwise [34,58]. Therefore, an Ising-type transition with the central charge $c = 1/2$ is expected at $|g_-| = |\tilde{g}_-|$, which corresponds to a free massless Majorana field. When K_- deviates slightly from $1/2$, a similar picture is still expected to hold as the change in K_- is a marginal perturbation. In the present argument, we have ignored perturbations which have larger scaling dimensions than the $g_\pm$ and $\tilde{g}$ terms in Eq. (9). If such terms also become relevant, they can potentially change the nature of the phase transitions. We will address this issue later.

We are ready to discuss the expected phase diagram of the model in Eq. (1). We assume that Δ is slightly larger than unity, i.e., in a weakly easy-axis regime. We fix the values of $J_\perp > 0$ and $\Delta > 1$, and vary $J_4 \geqslant 0$. We then find two phase transitions as follows. The first transition occurs at $J_{4,c}^{\rm Ising} \approx [(2b_0^2 - \Delta a_1^2)/(3d)^2]J_\perp$, which is an Ising-type transition with the central charge $c = 1/2$ in the antisymmetric channel. The second transition occurs at $J_{4,c}^{\rm Gauss} = \Delta(a_1/3d)^2 J_\perp$, which is a Gaussian-type transition with the central charge $c = 1$ in the symmetric channel. For $J_4 < J_{4,c}^{\rm Ising}$, the coupling constants in Eqs. (10) satisfy $g_+ > 0$ and $0 < g_- < \tilde{g}_-$, and the resulting state is characterized by the field locking at

$$(2\sqrt{2\pi}\phi_+, \sqrt{2\pi}\theta_-) = (\pi, \pi). \quad (11)$$

This corresponds to the RS phase, which is known in an antiferromagnetic ladder model [32–34]. For $J_{4,c}^{\rm Ising} < J_4 < J_{4,c}^{\rm Gauss}$, g_- becomes larger than $\tilde{g}_-$, resulting in the field locking at

$$2\sqrt{2\pi}(\phi_+, \phi_-) = (\pi, \mp\pi). \quad (12)$$

These correspond to the Néel phase with

$$\begin{aligned} \langle \mathcal{O}_{\rm Néel}(j)\rangle &= -(-1)^j a_1 \langle \sin(\sqrt{2\pi}\phi_+)\sin(\sqrt{2\pi}\phi_-)\rangle \\ &= \pm(-1)^j c_{\rm N}, \end{aligned} \quad (13)$$

where $\mathcal{O}_{\rm Néel}(j)$ is defined in Eq. (3) and $c_{\rm N} > 0$ is a constant independent of j. For $J_4 > J_{4,c}^{\rm Gauss}$, g_+ becomes negative, resulting in the field locking at

$$2\sqrt{2\pi}(\phi_+, \phi_-) = (0, \mp\pi). \quad (14)$$

These correspond to the SD phase with

$$\begin{aligned}\langle \mathcal{O}_{\rm SD}(j)\rangle &= -(-1)^j(3d)\langle \cos(\sqrt{2\pi}\phi_+)\sin(\sqrt{2\pi}\phi_-)\rangle \\ &= \pm(-1)^j c_{\rm SD}, \end{aligned} \tag{15}$$

where $\mathcal{O}_{\rm SD}(j)$ is defined in Eq. (4) and $c_{\rm SD} > 0$ is again a constant independent of j. In the isotropic limit $\Delta \to 1$, the two transition points $J_{4,c}^{\rm Ising}$ and $J_{4,c}^{\rm Gauss}$ merge into the single point $J_{4,c} = (\bar{a}/3\bar{d})^2 J_\perp$, at which the central charge is expected to be $c = 3/2$ [41–45,59]. In Ref. [45], this point was estimated to be $J_{4,c} = 2.05 J_\perp$ using the numerical values of $\bar{a}$ and $\bar{d}$ in the Heisenberg chain at a certain scale. More detailed phase diagrams in the $J_\perp$-J_4 plane in the isotropic case $\Delta = 1$ have been obtained numerically in Refs. [41,42].

In this paper, we are particularly interested in the nature of the transition between the Néel and SD phases. While the effective Hamiltonian in Eq. (9) suggests that this transition is likely to be of the Gaussian type, we have to examine whether possible perturbations to the theory can modify this scenario. Since the antisymmetric channel remains gapped at this transition, we can focus on the symmetric channel. As a possible perturbation, we can consider, for example, a higher-frequency cosine potential $\cos(4\sqrt{2\pi}\phi_+)$ with the scaling dimension $8K_+$. If this term becomes relevant, it can crucially change the nature of the phase transition [22]. With a negative coefficient, for example, this term has minima at $2\sqrt{2\pi}\phi_+ = 0$ and π, which correspond to the Néel and SD orders in Eqs. (12) and (14). Different signs of g_+ select different types of orders, and thus the first-order transition at $g_+ = 0$ separates the two phases. In our numerical results for $J_\perp = 1$ in Sec. IV, K_+ is estimated to be $K_+ \approx 0.6$ as shown in Table I, and thus the above higher-frequency cosine term is expected to be irrelevant.

In passing, we comment on the case of $J_\perp > 0$ and $J_4 < 0$, which has a closer form to the original J-Q model on a square lattice studied in Ref. [3]. In this case, the symmetric channel remains gapped as g_+ is always positive. An Ising transition in the antisymmetric channel occurs at $\tilde{J}_{4,c}^{\rm Ising} \approx -[(\Delta a_1^2 + 2b_0^2)/(3d)^2]J_\perp$ [45]. For $J_4 > \tilde{J}_{4,c}^{\rm Ising}$, we have $|g_-| < \tilde{g}_-$, which results in the RS phase with Eq. (11). For $J_4 < \tilde{J}_{4,c}^{\rm Ising}$, we have $g_- < -\tilde{g}_- < 0$, which results in the field locking at

$$2\sqrt{2\pi}(\phi_+, \phi_-) = (\pi, 2\pi),\ (\pi, 0). \tag{16}$$

These correspond to the CD phase with

$$\begin{aligned}\langle \mathcal{O}_{\rm CD}(j)\rangle &= \tfrac{1}{4}\langle \boldsymbol{S}_{1,j-1}\cdot\boldsymbol{S}_{1,j} + \boldsymbol{S}_{2,j-1}\cdot\boldsymbol{S}_{2,j} \\ &\quad - \boldsymbol{S}_{1,j}\cdot\boldsymbol{S}_{1,j+1} - \boldsymbol{S}_{2,j}\cdot\boldsymbol{S}_{2,j+1}\rangle \\ &= -(-1)^j(3d)\langle \sin(\sqrt{2\pi}\phi_+)\cos(\sqrt{2\pi}\phi_-)\rangle \\ &= \pm(-1)^j c_{\rm CD}, \end{aligned}$$

where $c_{\rm CD} > 0$ is a constant independent of j. We therefore have the RS-CD transition of an Ising type, which is robust against the introduction of the XXZ anisotropy. This is why we focus on the region of $J_\perp > 0$ and $J_4 > 0$ in our study of the Néel-VBS transition.

C. Critical properties around the Gaussian transition

Assuming that the Néel-SD transition is of the Gaussian type, we discuss the scaling behavior of physical quantities around this transition. We first consider the correlation functions of the Néel and dimer operators, $\mathcal{O}_{\rm Néel}(j)$ and $\mathcal{O}_{\rm SD}(j)$, at the transition point. As seen in the bosonized expressions in Eqs. (13) and (15), these operators involve both the fields $\phi_\pm$. As the symmetric channel is described by the Gaussian theory at the transition point, the symmetric component $\sin(\sqrt{2\pi}\phi_+)$ or $\cos(\sqrt{2\pi}\phi_+)$ shows a critical correlation with the decay exponent K_+. In contrast, as $\sqrt{2\pi}\phi_-$ remains locked at $\mp\pi/2$, the antisymmetric component $\sin(\sqrt{2\pi}\phi_-)$ shows a correlation that converges to a nonvanishing constant above a certain length scale proportional to the inverse of the excitation gap. Therefore, above this scale, the correlation functions in total exhibit the power-law behavior:

$$C_{\rm Néel}(r) := (-1)^r\langle \mathcal{O}_{\rm Néel}(r)\mathcal{O}_{\rm Néel}(0)\rangle \sim r^{-K_+}, \tag{17a}$$

$$C_{\rm SD}(r) := (-1)^r\langle \mathcal{O}_{\rm SD}(r)\mathcal{O}_{\rm SD}(0)\rangle \sim r^{-K_+}. \tag{17b}$$

Hence, the decay exponents $\eta_{\rm Néel}$ and $\eta_{\rm SD}$ of the two correlation functions are both equal to the TLL parameter K_+.

We next discuss the scaling behavior when the system deviates slightly from the critical point $J_{4,c}^{\rm Gauss}$. In this case, the dimensionless coupling constant $G_+ := g_+ a^2/(2\pi v) \propto (J_4 - J_{4,c})/J$ grows along the RG flow as $G(\ell) = G_+ e^{(2-2K_+)\ell}$ as the short-distance cutoff a is changed to $e^\ell a$. We continue the RG transformation until the running coupling constant $G_+(\ell)$ becomes $O(1)$. We suppose that the correlation length ξ is a constant ξ_0 in units of $e^\ell a$ for this ℓ. We then find

$$\xi \sim \xi_0 e^\ell a \sim |G_+|^{-\nu} \sim \left|J_4 - J_{4,c}^{\rm Gauss}\right|^{-\nu}, \tag{18}$$

with the exponent

$$\nu = \frac{1}{2 - 2K_+}. \tag{19}$$

In the Néel phase ($J_4 < J_{4,c}^{\rm Gauss}$), the correlation function $C_{\rm Néel}(r)$ shows the power-law behavior in Eq. (17a) below the scale of ξ and converges to a nonvanishing constant above this scale. This means that the Néel order parameter acquires a nonzero expectation value,

$$(-1)^j\langle \mathcal{O}_{\rm Néel}(j)\rangle \sim \pm\sqrt{\xi^{-K_+}} \sim \pm\left(J_{4,c}^{\rm Gauss} - J_4\right)^\beta, \tag{20}$$

with the exponent

$$\beta = \frac{\nu K_+}{2} = \frac{K_+}{4 - 4K_+}. \tag{21}$$

Likewise, in the SD phase ($J_4 > J_{4,c}^{\rm Gauss}$), the dimer order parameter acquires a nonzero expectation value,

$$(-1)^j\langle \mathcal{O}_{\rm SD}(j)\rangle \sim \pm\left(J_4 - J_{4,c}^{\rm Gauss}\right)^\beta, \tag{22}$$

with the same exponent β as above.

All the critical exponents, β, ν, and $\eta_{\rm Néel/SD}$ discussed above are obtained as functions of the single TLL parameter K_+. As K_+ in general varies continuously along the phase boundary, these critical exponents also vary accordingly.

IV. NUMERICAL ANALYSIS OF THE NÉEL-SD TRANSITION

A. Method

We have performed numerical calculations directly for the infinite system by using the VUMPS algorithm [23,24]. In this algorithm, a variational state is prepared in the form of a uniform MPS by assuming the translational invariance, and the ground state is obtained by iteratively optimizing the constituent tensors to lower the variational energy.

The original VUMPS is an algorithm for 1D chains. It can be applied to the present ladder system by regarding two sites on each rung as a single effective site with the local Hilbert space dimension of four. We have adopted the two-site unit cell implementation in Ref. [23] as all phases discussed in Secs. II and III have the unit cell consisting of at most two effective sites (i.e., two rungs). We omit data points that do not converge sufficiently and use the data points that have the gradient norm $\|B\| < 10^{-10}$, where B is defined as the gradient of energy per site with respect to the elementary tensor in VUMPS.

B. Correlation length and entanglement entropy

We fix $J = J_\perp = 1$ and present the numerically obtained phase diagram in the J_4-Δ plane in Fig. 3. Below we study the Néel-SD transition along the red solid line ($\Delta = 1.2$) shown in Fig. 3 as a representative case.

We extract the correlation length ξ from the MPS with the finite bond dimension χ. In the case of two-site unit cells, the transfer matrix T is defined in the following way. We cast two-site unit cells into the single-site unit cells by

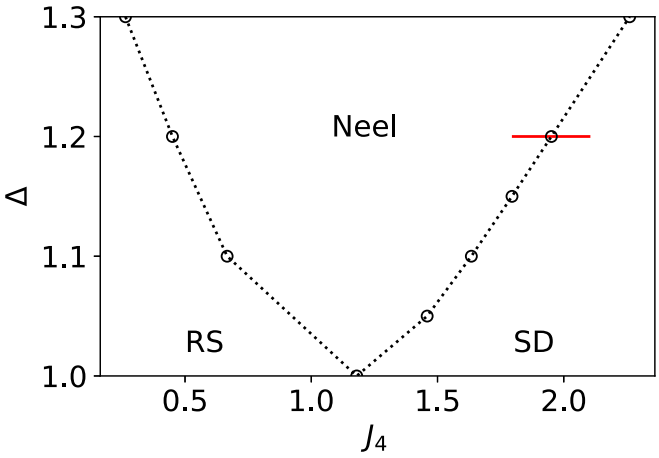

FIG. 3. Phase diagram of the model in Eq. (1) on the J_4-Δ plane with $J = J_\perp = 1$. The circles (○) indicate the transition points obtained through the analysis of the correlation length as shown in Fig. 4. The dotted lines are our assumption of the phase boundaries. We will focus on the phase transition along the red solid line with $\Delta = 1.2$ in Sec. IV. The numerical analysis of the RS-Néel transition is described in Appendix A. The transition point $J_{4,c} \simeq 1.19$ in the isotropic case $\Delta = 1$ has been obtained by the exact diagonalization [41]. We also obtained the same critical point within the error bar of bond dimension extrapolation by VUMPS, as described in Appendix B.

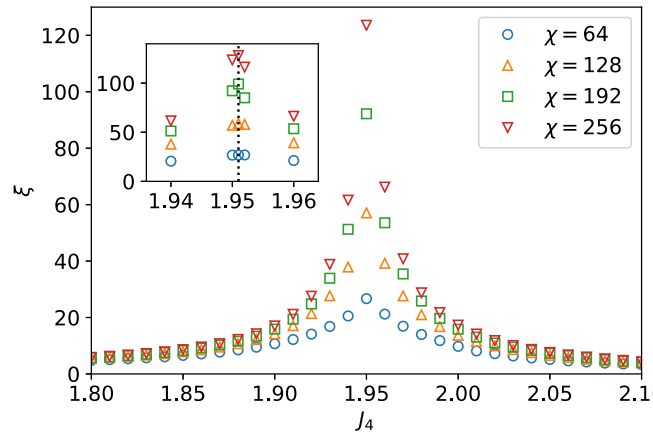

FIG. 4. Correlation length ξ as a function of J_4 around the Néel-SD transition for $\Delta = 1.2$ (see the red solid line in Fig. 3). The correlation length shows a sharp peak, which grows consistently with an increase in χ. In the case of $\chi = 256$, the peak of the correlation length exceeds 100 lattice spacings. These results are indicative of a continuous phase transition. We estimate the critical point to be $J_{4,c} = 1.951(1)$ as shown in the inset.

introducing $\mathbb{A}^s := A(1)^{s_1}A(2)^{s_2}$, where $A(k)^{s_k} \in \mathbb{R}^{\chi\times\chi}$ is the original matrix for the state s_k at the kth effective site and $\mathbb{A}^s \in \mathbb{R}^{\chi\times\chi}$ is the combined matrix for the state $s = (s_1, s_2)$. The transfer matrix T is then defined by $T := \sum_s \mathbb{A}^{s\dagger} \otimes \mathbb{A}^s$. The correlation length is calculated as $\xi(\chi) = -2/\ln|\lambda_2(\chi)|$, where $\lambda_2(\chi)$ is the second largest absolute eigenvalue of the transfer matrix. This method underestimates the correlation length when the bond dimension χ is finite. We plot the correlation length $\xi(\chi)$ at $\Delta = 1.2$ in Fig. 4. It shows that the correlation length has a sharp peak with consistent growth with an increase in χ. In particular, the peak of the correlation length $\xi(\chi)$ exceeds 100 lattice spacings in the case of $\chi = 256$. These results are indicative of a continuous phase transition with a diverging correlation length.

The critical point $J_{4,c} = 1.951(1)$ is obtained from the peak of the correlation length as shown in the inset of Fig. 4. We note that the error in this estimation is not a statistical one but is based on the observation that the correlation length at $J_4 = 1.951$ is larger than those at $J_4 = 1.950$ and $J_4 = 1.952$ irrespective of the bond dimension χ.

Critical points of a large class of 1D quantum systems are described by the conformal field theory (CFT). A convenient quantity for probing the underlying CFT is the entanglement entropy S. We calculate it for a bipartition of the infinite 1D system into two half-infinite chains. According to the CFT, the entanglement entropy S and the correlation length ξ have the relationship

$$S = \frac{c}{6}\ln\xi + S_0, \tag{23}$$

where c is the central charge and S_0 is a constant [60,61]. Figure 5 shows that S and ξ at $J_4 = 1.951$ are well fitted by Eq. (23) with $c \simeq 1.02$. This result is also indicative of a continuous phase transition because S and ξ do not follow Eq. (23) if the transition is a discontinuous one. This result is consistent with the Gaussian transition with $c = 1$ suggested by the effective field theory.

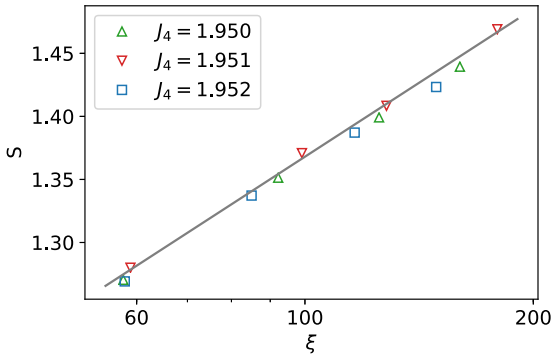

FIG. 5. Entanglement entropy $S(\chi)$ versus the correlation length $\xi(\chi)$ for the bond dimensions $\chi = 128, 192, 256, 320$. These are calculated at three points near the Néel-SD transition point for $\Delta = 1.2$. A logarithmic scale is used for the horizontal axis. The gray straight line shows the CFT formula in Eq. (23) with $c \simeq 1.02$ and $S_0 \simeq 0.59$, which is the result of a fitting to the case of $J_4 = 1.951$.

C. Critical exponents

We proceed to analyze the critical exponents around the estimated critical point $J_{4,c}$. First, we calculate the correlation length exponents $\nu_\pm$. Near the critical point, the correlation length ξ is expected to obey the scaling

$$\xi = \begin{cases} \xi_-(J_{4,c} - J_4)^{-\nu_-} & (J_4 < J_{4,c}) \\ \xi_+(J_4 - J_{4,c})^{-\nu_+} & (J_4 > J_{4,c}), \end{cases} \tag{24}$$

where $\nu_\pm$ are the critical exponents and $\xi_\pm$ are the amplitudes in the Néel $(-)$ and SD $(+)$ phases. In the numerical result shown in Fig. 6, we find a linear relation between $\ln(1/\xi)$ and $\ln \Delta J_4$, where $\Delta J_4 := |J_4 - J_{4,c}|$. It also shows that when ΔJ_4 is large, the correlation length ξ does not follow Eq. (24). By using the region where the data points follow Eq. (24), we obtain $\nu_- = 1.13(11)$ and $\nu_+ = 1.26(16)$. In these estimates, we have also taken account of a possible error in the estimate of the transition point $J_{4,c}$ as described in Appendix C. In Fig. 6, we observe that when approaching the transition point, the correlation length ξ in the Néel and SD phases tends to collapse onto the same curve. This suggests that both the exponents $\nu_\pm$ and the amplitudes $\xi_\pm$ are equal between the two sides, as expected for a Gaussian transition; see Eq. (18).

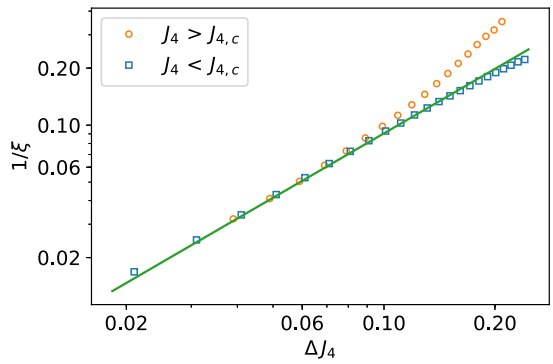

FIG. 6. Power-law scaling behavior of the correlation length ξ as a function of $\Delta J_4 := |J_4 - J_{4,c}|$ around the Néel-SD transition point $J_{4,c} = 1.951$ for $\Delta = 1.2$. Logarithmic scales are used for both axes. For each J_4, the correlation length ξ has been extrapolated to infinite χ as described in Appendix C, and the present figure shows the extrapolated values. By using the region where the data points follow Eq. (24), we obtain $\nu_- = 1.13(11)$ and $\nu_+ = 1.26(16)$ in the Néel $(J_4 < J_{4,c})$ and SD $(J_4 > J_{4,c})$ phases, respectively. The data in the two phases tend to collapse onto the same curve when approaching the critical point. The solid line is a guide to the eye and its slope is 1.13.

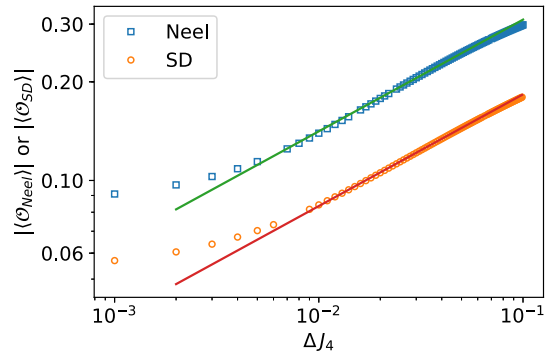

FIG. 7. Power-law scaling behavior [Eq. (25)] of the Néel and SD order parameters [defined in Eqs. (3) and (4)] around the transition point $J_{4,c} = 1.951$ for $\Delta = 1.2$. Logarithmic scales are used for both axes. The calculations are performed with the bond dimension $\chi = 256$. The order parameter exponents are estimated to be $\beta_{\text{Néel}} = 0.34(3)$ and $\beta_{\text{SD}} = 0.34(3)$ as described in Appendix D. The two solid parallel lines are guides to the eye and their slope is 0.34.

Second, we calculate the order parameter critical exponents $\beta_{\text{Néel}}$ and β_{SD}. Near the critical point, the order parameters defined in Eqs. (3) and (4) are expected to obey the scaling

$$(-1)^j \langle \mathcal{O}_{\text{Néel/SD}}(j) \rangle = \begin{cases} \pm A_{\text{Néel/SD}} \, (\Delta J_4)^{\beta_{\text{Néel/SD}}} & \text{(Néel/SD phase)} \\ 0 & \text{(otherwise)}, \end{cases} \tag{25}$$

where $A_{\text{Néel/SD}}$ are constants. Numerical data of the order parameters are shown in Fig. 7, where we find a linear relation between $\ln |\langle \mathcal{O}_{\text{Néel/SD}} \rangle|$ and $\ln(\Delta J_4)$. We also find that when ΔJ_4 is large or small, the order parameters do not follow Eq. (25). By using the region where the data points follow Eq. (25), we obtain $\beta_{\text{Néel}} = 0.34(3)$ and $\beta_{\text{SD}} = 0.34(3)$. The details of the calculation are described in Appendix D.

Lastly, we calculate the correlation functions to determine the exponents $\eta_{\text{Néel}}$ and η_{SD}. As seen in Eqs. (17), the correlation functions of the Néel and dimer operators are expected to show a power-law decay at the critical point,

$$C_{\text{Néel/SD}}(r) = C^{(0)}_{\text{Néel/SD}} r^{-\eta_{\text{Néel/SD}}}, \tag{26}$$

where $C^{(0)}_{\text{Néel/SD}}$ are constants. Figure 8 presents the correlation functions calculated for $J_4 = 1.950$ and 1.952, which are close to the Néel-SD transition point. The Néel (SD) correlation function plotted in logarithmic scales is bent upward (downward) for $J_4 = 1.950$ and downward (upward) for $J_4 = 1.952$, indicating that the transition point is located between them in accord with the analysis of the correlation length in Fig. 5. Although the two points $J_4 = 1.950$ and 1.952 deviate slightly from the critical point, the correlation functions are expected

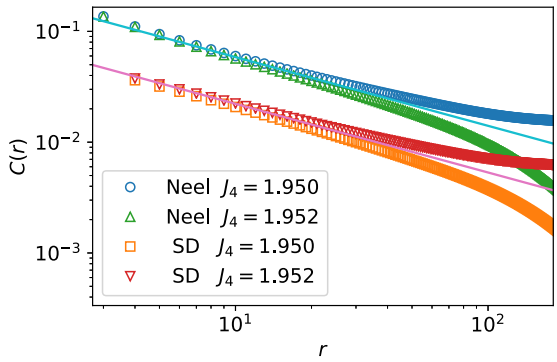

FIG. 8. Néel and SD correlation functions at two points near the Néel-SD transition point $J_{4,c} = 1.951(1)$ for $\Delta = 1.2$. Logarithmic scales are used for both axes. The calculations are performed with $\chi = 210$. The critical exponents are estimated to be $\eta_{\text{Néel}} = 0.63(6)$ and $\eta_{\text{SD}} = 0.61(5)$. The two parallel solid lines are guides to the eye and their slope is -0.62.

to show a power-law behavior [Eq. (26)] below the scale of the correlation length. This can be confirmed via an approximately linear behavior at relatively short distances in Fig. 8. The exponents $\eta_{\text{Néel/SD}}$ at the critical point should then exist between the slopes of the linear behaviors for $J_4 = 1.950$ and 1.952. For the Néel correlation function, the slopes at $J_4 = 1.950$ and 1.952 are estimated to be -0.572 and -0.684, respectively, using the region $7 < r < 34$. We therefore estimate the critical exponent as $\eta_{\text{Néel}} = 0.63(6)$. In the same way, we obtain $\eta_{\text{SD}} = 0.61(5)$.

As summarized in Table I, we have estimated the Néel-SD transition points and the critical exponents in a similar manner for some values of Δ. We can confirm the relations $\beta_{\text{Néel}} = \beta_{\text{SD}}(=: \beta)$, $\nu_- = \nu_+(=: \nu)$, and $\eta_{\text{Néel}} = \eta_{\text{SD}}(=: \eta)$ within numerical accuracy. We can further confirm the consistency with the constraints

$$\beta = \frac{\eta}{4 - 4\eta}, \quad \nu = \frac{1}{2 - 2\eta}, \tag{27}$$

which are expected for the Gaussian universality class as discussed in Sec. III C. For example, the substitution of $\eta_{\text{Néel}} = 0.63(6)$ (the estimate for $\Delta = 1.20$) into Eqs. (27) gives $\beta = 0.44(11)$ and $\nu = 1.38(22)$, which are consistent with the estimates of $\beta_{\text{Néel/SD}}$ and $\nu_\pm$ in Table I within numerical accuracy. Our numerical results thus support the scenario that the Néel-SD transition belongs to the Gaussian universality class. However, the exponents in Table I do not detectably change along the phase boundary while they are in general allowed to do so for the Gaussian class. To detect possible changes in the exponent along the phase boundary, calculations with larger bond dimensions χ would be required.

V. CONCLUSION

In this paper, we have studied the spin-1/2 two-leg XXZ ladder system with a four-spin interaction, which can be viewed as a 1D variant of the J-Q model on a square lattice. We have determined the phase diagram and analyzed the nature of the quantum phase transitions by means of VUMPS calculations for the infinite system and an effective field theory based on bosonization. We have presented evidence that the Néel-SD (VBS) transition belongs to the Gaussian universality class and the RS-Néel transition belongs to the $(1 + 1)$-dimensional Ising universality class.

In particular, we have conducted detailed analyses of the Néel-SD transition, which occurs between two ordered phases breaking different $\mathbb{Z}_2$ symmetries. The effective Hamiltonian [see Eq. (9)] for weak interchain couplings $|J_\perp|, |J_4| \ll J$ indicates that this transition is described by a sine-Gordon model in the symmetric channel and is likely to be of the Gaussian type. However, it is not obvious whether possible perturbations to the effective Hamiltonian can modify the scenario or whether the effective Hamiltonian is applicable when $J_\perp$ and J_4 are comparable to J. For these reasons, we numerically studied the Néel-SD transition. The VUMPS study is consistent with the expected Gaussian universality class. The correlation length shows a sharp peak that consistently grows with an increase in χ. By using the entanglement entropy, it turned out that the transition has the expected central charge $c = 1$. The numerically estimated critical exponents in Table I satisfy the relations $\beta_{\text{Néel}} = \beta_{\text{SD}}$, $\nu_- = \nu_+$, and $\eta_{\text{Néel}} = \eta_{\text{SD}}$ within numerical accuracy in consistency with the Gaussian transition, more generally, the emergent symmetry scenario [62,63] (the correlation length in Fig. 6 further suggests the equal amplitudes $\xi_- = \xi_+$). Furthermore, these exponents are consistent, within numerical accuracy, with the constraints in Eqs. (27) expected for the Gaussian universality class. The TLL parameter K_+ in the symmetric channel discussed in Sec. III is equal to the exponent $\eta_{\text{Néel/SD}}$, whose value is approximately 0.6 in Table I. Thus, the higher-frequency cosine potential with the scaling dimension $8K_+$ discussed in Sec. III B is expected to be irrelevant, lending further support to the scenario of the Gaussian transition. The critical exponents in Table I do not detectably change along the phase boundary while they are allowed to do so for the Gaussian class.

To reveal the relationship between our 1D J-Q-like model and the 2D J-Q model, it would be interesting to investigate

TABLE I. Numerical estimates of the critical point $J_{4,c}$ and the exponents $\beta_{\text{Néel/SD}}$, $\nu_\pm$, and $\eta_{\text{Néel/SD}}$ at several points along the Néel-SD phase boundary in Fig. 3.

Δ	$J_{4,c}$	$\beta_{\text{Néel}}$	β_{SD}	ν_-	ν_+	$\eta_{\text{Néel}}$	η_{SD}
1.05	1.459(1)	0.35(2)	0.36(3)	1.09(14)	1.15(10)	0.61(4)	0.60(3)
1.1	1.634(1)	0.35(2)	0.35(2)	1.13(10)	1.20(10)	0.61(4)	0.62(4)
1.15	1.795(1)	0.34(2)	0.35(2)	1.11(8)	1.19(11)	0.62(4)	0.61(4)
1.20	1.951(1)	0.34(3)	0.34(3)	1.13(11)	1.26(16)	0.63(6)	0.61(5)
1.30	2.261(1)	0.34(3)	0.34(3)	1.02(22)	1.19(13)	0.66(7)	0.60(6)

the dependence on the number of legs by studying, e.g., three- and four-leg ladder systems. It would also be interesting to study the Néel-SD transition in the 2D J-Q model with a positive coefficient $-Q > 0$ in the four-spin interaction, for which the QMC suffers from a sign problem but tensor network algorithms could be applicable.

ACKNOWLEDGMENTS

The authors would like to thank Y. Fuji, A. Furusaki, S. Iino, R. K. Kaul, H. Kohshiro, K. Tamai, and L. Vanderstraeten for stimulating discussions. This research was supported by JSPS KAKENHI Grants No. JP18K03446, No. JP19H01809, and No. JP20K03780, and by MEXT as Priority Issue on Post-K computer (Creation of New Functional Devices and High-Performance Materials to Support Next-Generation Industries) and Exploratory Challenge on Post-K Computer (Challenge of Basic Science—Exploring Extremes through Multi-Physics and Multi-Scale Simulations). The numerical computations were performed on computers at the Supercomputer Center, the Institute for Solid State Physics (ISSP), the University of Tokyo.

APPENDIX A: NUMERICAL ANALYSIS OF THE RS-NÉEL TRANSITION

In this Appendix, we describe our numerical results on the RS-Néel transition. We fix $J = J_\perp = 1$ and study the transition at $\Delta = 1.1$ as a representative case. The procedure is similar to our analysis of the Néel-SD transition in Sec. IV.

By analyzing the correlation length and the entanglement entropy, we obtain the critical point $J_{4,c} \simeq 0.666$ and the central charge $c \simeq 0.48$. Around the transition point, the correlation length shows consistent growth as a function of χ, which indicates a continuous nature of the transition. The critical exponents are estimated to be $\beta \simeq 0.12$, $\nu_- \simeq 1.0$, $\nu_+ \simeq 1.0$, and $\eta \simeq 0.26$.

The above numerical results are consistent with the $(1+1)$-dimensional Ising universality class with $c = 1/2$, $\beta = 1/8$, $\nu = 1$, and $\eta = 1/4$. We note that the occurrence of an Ising transition is also suggested by the field-theoretical analysis in Sec. III. We have obtained similar results on other points along the boundary between the RS and Néel phases.

APPENDIX B: NUMERICAL ANALYSIS OF THE RS-SD TRANSITION IN THE ISOTROPIC CASE

In this Appendix, we describe our numerical results on the RS-SD transition in the isotropic case $\Delta = 1$ with $J = J_\perp = 1$ and $J_4 \simeq 1.19$. The previous study based on exact diagonalization [41] has suggested that this transition is described by the $SU(2)_2$ WZW model with $c = 3/2$. Below we show that our VUMPS results are consistent with the previous study.

The correlation length ξ calculated by VUMPS around the expected RS-SD transition exhibits two kinks instead of a single sharp peak as shown in Fig. 9. In the intermediate region between the two kinks, the Néel order parameter $\langle \mathcal{O}_{\text{Néel}} \rangle$ has been found to be nonzero (not shown). As the antiferromagnetic order that spontaneously breaks the SU(2) symmetry is not likely to appear in the present ladder system

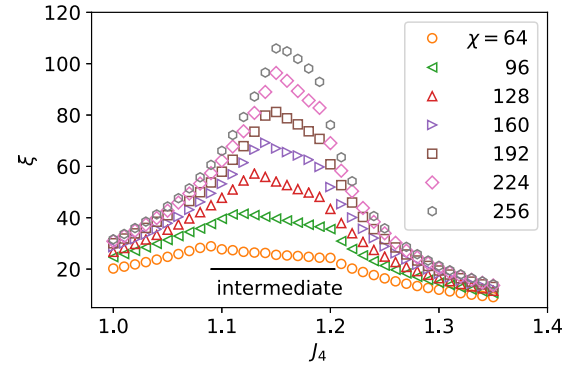

FIG. 9. Correlation length ξ as a function of J_4 around the expected RS-SD transition in the isotropic case $\Delta = 1$. The correlation length grows consistently with an increase in χ, but the correlation length for fixed χ exhibits two kinks instead of a single sharp peak. The intermediate region between the two kinks tends to shrink with an increase in χ, as we analyze more closely in Fig. 10.

(because of the theorem in Ref. [15]), the intermediate region with $\langle \mathcal{O}_{\text{Néel}} \rangle \neq 0$ can be considered an artifact of the present numerical method whose accuracy is controlled by the bond dimension χ. With an increase in χ, the intermediate region indeed tends to shrink, and the correlation length ξ around this region continues to increase, as seen in Fig. 9. The extrapolation of the intermediate region to infinite χ shown in Fig. 10 is consistent with the vanishing of this region within numerical accuracy. These results are indicative of a direct continuous transition between the RS and SD phases in the isotropic case. Assuming this is true, we obtain the central charge $c \simeq 1.55$ by fitting Eq. (23) to the data of the entanglement entropy versus the correlation length, as shown in Fig. 11.

APPENDIX C: ESTIMATION OF THE CORRELATION LENGTH EXPONENTS

In this Appendix, we describe how we estimate the correlation length critical exponents $\nu_\pm$ and their error ranges. First, for given Δ, we extrapolate the correlation length to infinite χ at each J_4. Second, we determine the region that is used for the fitting. Finally, we fit the scaling form in Eq. (24) to the selected data points. As an example, we explain the procedure

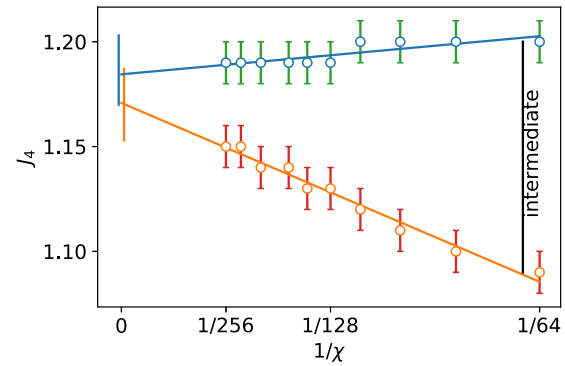

FIG. 10. Dependence of the intermediate region found in Fig. 9 on the bond dimension χ. The extrapolation to infinite χ is consistent with the vanishing of this region within numerical accuracy.

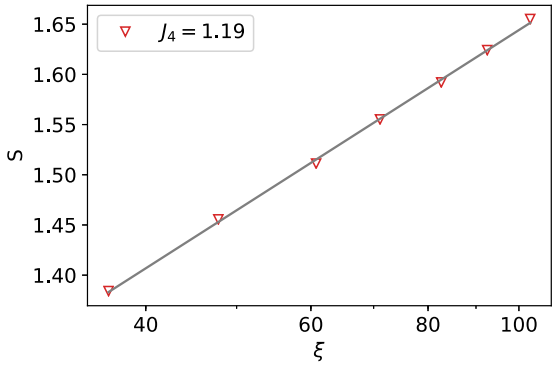

FIG. 11. Entanglement entropy $S(\chi)$ versus the correlation length $\xi(\chi)$ for the bond dimension $\chi = 96, 128, 160, 192, 224, 256, 280$. These are calculated in the isotropic case $\Delta = 1$ with $J = J_\perp = 1$ and $J_4 = 1.19$, around which the transition between the RS and SD phases is expected to occur. A logarithmic scale is used for the horizontal axis. The gray straight line shows the CFT formula Eq. (23) with $c \simeq 1.55$ and $S_0 \simeq 0.45$, which is the result of a fitting to the numerical data.

by taking the Néel-SD transition for $\Delta = 1.2$ as shown in Fig. 6.

As discussed in Sec. IV B, we tend to underestimate the correlation length when we use the transfer matrix with the finite bond dimension χ. Since this underestimation is not limited to the critical point, we need to perform an appropriate extrapolation to infinite χ at each point. Several extrapolation methods for 1D systems are known [64]. In these methods, $1/\xi$ is regarded as a linear function of $1/\chi$ or $|\lambda_2 - \lambda_3|$, where λ_2 and λ_3 are the second and third largest absolute eigenvalues of the transfer matrix. However, we cannot use these methods directly because our model is a ladder system and its transfer matrix has a different eigenvalue distribution from those of 1D chains. We instead use the linear scaling of the correlation length $\xi(\chi)$ with $1/\sqrt{\chi}$. The reason why we use $\sqrt{\chi}$ instead of χ is as follows. When we have two independent chains, each of which is described by a uniform MPS with the bond dimension $\sqrt{\chi}$, where we assume that χ is a square number, the whole system is a two-leg ladder system without interchain couplings and is described by a uniform MPS with χ. In this case, the relationship between ξ and χ in the two-leg ladder is the same as the relationship between ξ and $\sqrt{\chi}$ in 1D chains. We assume that the above discussion is applicable to our system having interchain couplings. This method is not suitable near the critical point because the correlation length at the critical point has been predicted to follow $\xi \propto \chi^\kappa$, where $\kappa = 6/[c(\sqrt{12/c} + 1)]$ with c being the central charge [61,65]. To estimate a possible error in $\nu_\pm$, we assume that the extrapolated correlation length $\xi(\chi \to \infty)$ has its error at worst 5% in our two-leg ladder model [66]. Note that the error is not a statistical one but a systematic one.

Next, we determine the fitting region. At $\Delta = 1.2$, we first fix the critical point at $J_{4,c} = 1.951$, which is determined in Sec. IV B. As discussed above, we cannot use the data points near the critical point because the estimated correlation length has a larger error there. Additionally, we cannot use the data points that are far from the critical point. This is because they do not follow the power-law scaling as shown in Fig. 6. By fitting the scaling form Eq. (24) to the selected data points, we obtain $\nu_- = 1.12 \pm 0.09$ and $\nu_+ = 1.25 \pm 0.14$. However, the errors in these results do not include the effect of a possible error in the critical point and would be underestimated. To estimate the error more reliably, we have to take into account the error in the critical point $J_{4,c}$. Thus, we repeat the same procedure assuming that the critical point is $J_{4,c} = 1.950$ and $J_{4,c} = 1.952$. The results are shown in Table II. Thus, we conclude that $\nu_- = 1.13(11)$ and $\nu_+ = 1.26(16)$.

TABLE II. Numerical estimates of the critical exponents $\nu_\pm$ for the Néel-SD transition with different values of the assumed transition point $J_{4,c}$. The case of $J_{4,c} = 1.951$ corresponds to Fig. 6.

Assumed $J_{4,c}$	ν_-	ν_+
1.950	1.10(8)	1.27(14)
1.951	1.12(9)	1.25(14)
1.952	1.15(9)	1.24(14)

APPENDIX D: ESTIMATION OF THE ORDER PARAMETER EXPONENTS

In this Appendix, we describe how we estimate the order parameter critical exponents $\beta_{\text{Néel/SD}}$ and their error ranges. The procedure is essentially the same as the estimation of the correlation length exponents $\nu_\pm$ in Appendix C. Here, we fit the scaling form Eq. (25) to the selected data points.

As shown in Fig. 7, we observe a kink at $\Delta J_4 \sim 0.008$ for both order parameters. We tend to overestimate the order parameters near the critical point ($\Delta J_4 < 0.008$) because χ is not large enough. To estimate the gap between the order parameter $\langle \mathcal{O}(\chi = 256) \rangle$ and the exact one, we extrapolate the order parameter by fitting the data points with a function

$$f(\chi) = a + b\left(\frac{1}{\chi}\right)^c, \tag{D1}$$

where a, b, and $c > 1$ are fitting parameters. We confirm that $f(\chi \to \infty) = a$ almost always underestimates the order parameter by comparing the extrapolated order parameter with the exact one in the transverse-field Ising chain. Thus, we expect that the exact order parameter is between $\langle \mathcal{O}(\chi = 256) \rangle$ and $f(\chi \to \infty)$. The error of the order parameter is estimated to be smaller than

$$\Delta\langle \mathcal{O}(\chi = 256) \rangle := \frac{|\langle \mathcal{O}(\chi = 256) \rangle - f(\chi \to \infty)|}{|\langle \mathcal{O}(\chi = 256) \rangle|}. \tag{D2}$$

Next, we need to determine the fitting region. We fix the critical point at $J_{4,c} = 1.951$, which is determined in

TABLE III. Numerical estimates of the critical exponents $\beta_{\text{Néel/SD}}$ for the Néel-SD transition with different values of the assumed transition point $J_{4,c}$. The case of $J_{4,c} = 1.951$ corresponds to Fig. 7.

Assumed $J_{4,c}$	$\beta_{\text{Néel}}$	β_{SD}
1.950	0.329(18)	0.352(18)
1.951	0.338(18)	0.342(17)
1.952	0.347(19)	0.331(17)

Sec. IV B, We choose the data points with $\Delta\langle\mathcal{O}(\chi = 256)\rangle < 10^{-2}$ and discard the data points that are far from the critical point because they do not follow the power-law scaling in Eq. (25) as shown in Fig. 7. By fitting the scaling form in Eq. (25) to the selected data points, we obtain $\beta_{\text{Néel}} = 0.338(18)$ and $\beta_{\text{SD}} = 0.342(17)$ with the estimated critical point $J_{4,c} = 1.951$, assuming that all data points have 1% systematic error. In the same way, we obtain the critical exponents in Table III. As a result, we obtain $\beta_{\text{Néel}} = 0.34(3)$ and $\beta_{\text{SD}} = 0.34(3)$.

[1] T. Senthil, A. Vishwanath, L. Balents, S. Sachdev, and M. P. A. Fisher, Deconfined quantum critical points, Science **303**, 1490 (2004).

[2] T. Senthil, L. Balents, S. Sachdev, A. Vishwanath, and M. P. A. Fisher, Quantum criticality beyond the Landau-Ginzburg-Wilson paradigm, Phys. Rev. B **70**, 144407 (2004).

[3] A. W. Sandvik, Evidence for Deconfined Quantum Criticality in a Two-Dimensional Heisenberg Model with Four-Spin Interactions, Phys. Rev. Lett. **98**, 227202 (2007).

[4] F.-J. Jiang, M. Nyfeler, S. Chandrasekharan, and U.-J. Wiese, From an antiferromagnet to a valence bond solid: Evidence for a first-order phase transition, J. Stat. Mech. (2008) P02009.

[5] A. B. Kuklov, M. Matsumoto, N. V. Prokof'ev, B. V. Svistunov, and M. Troyer, Deconfined Criticality: Generic First-Order Transition in the SU(2) Symmetry Case, Phys. Rev. Lett. **101**, 050405 (2008).

[6] K. Harada, T. Suzuki, T. Okubo, H. Matsuo, J. Lou, H. Watanabe, S. Todo, and N. Kawashima, Possibility of deconfined criticality in SU(N) heisenberg models at small N, Phys. Rev. B **88**, 220408(R) (2013).

[7] S. Jiang and O. Motrunich, Ising ferromagnet to valence bond solid transition in a one-dimensional spin chain: Analogies to deconfined quantum critical points, Phys. Rev. B **99**, 075103 (2019).

[8] B. Roberts, S. Jiang, and O. I. Motrunich, Deconfined quantum critical point in one dimension, Phys. Rev. B **99**, 165143 (2019).

[9] C. Mudry, A. Furusaki, T. Morimoto, and T. Hikihara, Quantum phase transitions beyond Landau-Ginzburg theory in one-dimensional space revisited, Phys. Rev. B **99**, 205153 (2019).

[10] G. Sun, B.-B. Wei, and S.-P. Kou, Fidelity as a probe for a deconfined quantum critical point, Phys. Rev. B **100**, 064427 (2019).

[11] Q. Luo, J. Zhao, and X. Wang, Intrinsic jump character of first-order quantum phase transitions, Phys. Rev. B **100**, 121111(R) (2019).

[12] R.-Z. Huang, D.-C. Lu, Y.-Z. You, Z. Y. Meng, and T. Xiang, Emergent symmetry and conserved current at a one-dimensional incarnation of deconfined quantum critical point, Phys. Rev. B **100**, 125137 (2019).

[13] P. Patil, E. Katz, and A. W. Sandvik, Numerical investigations of SO(4) emergent extended symmetry in spin-$\frac{1}{2}$ Heisenberg antiferromagnetic chains, Phys. Rev. B **98**, 014414 (2018).

[14] B. Roberts, S. Jiang, and O. I. Motrunich, One-dimensional model for deconfined criticality with $\mathbb{Z}_3 \times \mathbb{Z}_3$ symmetry, arXiv:2010.07917.

[15] T. Momoi, Quantum fluctuations in quantum lattice systems with continuous symmetry, J. Stat. Phys. **85**, 193 (1996).

[16] S. Yang, D.-X. Yao, and A. W. Sandvik, Deconfined quantum criticality in spin-1/2 chains with long-range interactions, arXiv:2001.02821.

[17] F. D. M. Haldane, Spontaneous dimerization in the $S = \frac{1}{2}$ Heisenberg antiferromagnetic chain with competing interactions, Phys. Rev. B **25**, 4925 (1982).

[18] I. Affleck and F. D. M. Haldane, Critical theory of quantum spin chains, Phys. Rev. B **36**, 5291 (1987).

[19] K. Kuboki and H. Fukuyama, Spin-Peierls transition with competing interactions, J. Phys. Soc. Jpn. **56**, 3126 (1987).

[20] K. Nomura and K. Okamoto, Phase diagram of $S = 1/2$ XXZ chain with next-nearest-neighbor interaction, J. Phys. Soc. Jpn. **62**, 1123 (1993).

[21] K. Nomura and K. Okamoto, Critical properties of $S = 1/2$ antiferromagnetic XXZ chain with next-nearest-neighbour interactions, J. Phys. A: Math. Gen. **27**, 5773 (1994).

[22] S. Furukawa, M. Sato, and A. Furusaki, Unconventional néel and dimer orders in a spin-$\frac{1}{2}$ frustrated ferromagnetic chain with easy-plane anisotropy, Phys. Rev. B **81**, 094430 (2010).

[23] V. Zauner-Stauber, L. Vanderstraeten, M. T. Fishman, F. Verstraete, and J. Haegeman, Variational optimization algorithms for uniform matrix product states, Phys. Rev. B **97**, 045145 (2018).

[24] L. Vanderstraeten, J. Haegeman, and F. Verstraete, Tangent-space methods for uniform matrix product states, SciPost Phys. Lect. Notes 7 (2019).

[25] A. Läuchli, J. C. Domenge, C. Lhuillier, P. Sindzingre, and M. Troyer, Two-Step Restoration of SU(2) Symmetry in a Frustrated Ring-Exchange Magnet, Phys. Rev. Lett. **95**, 137206 (2005).

[26] A. Sen and A. W. Sandvik, Example of a first-order Néel to valence-bond-solid transition in two dimensions, Phys. Rev. B **82**, 174428 (2010).

[27] A. Banerjee, K. Damle, and A. Paramekanti, Néel to staggered dimer order transition in a generalized honeycomb lattice Heisenberg model, Phys. Rev. B **83**, 134419 (2011).

[28] C. Xu and L. Balents, Quantum phase transitions around the staggered valence-bond solid, Phys. Rev. B **84**, 014402 (2011).

[29] R. Orús, A practical introduction to tensor networks: Matrix product states and projected entangled pair states, Ann. Phys. **349**, 117 (2014).

[30] J. Jordan, R. Orús, G. Vidal, F. Verstraete, and J. I. Cirac, Classical Simulation of Infinite-Size Quantum Lattice Systems in Two Spatial Dimensions, Phys. Rev. Lett. **101**, 250602 (2008).

[31] H. C. Jiang, Z. Y. Weng, and T. Xiang, Accurate Determination of Tensor Network State of Quantum Lattice Models in two Dimensions, Phys. Rev. Lett. **101**, 090603 (2008).

[32] S. P. Strong and A. J. Millis, Competition between Singlet Formation and Magnetic Ordering in One-Dimensional Spin Systems, Phys. Rev. Lett. **69**, 2419 (1992).

[33] S. P. Strong and A. J. Millis, Competition between singlet formation and magnetic ordering in one-dimensional spin systems, Phys. Rev. B **50**, 9911 (1994).

[34] D. G. Shelton, A. A. Nersesyan, and A. M. Tsvelik, Antiferromagnetic spin ladders: Crossover between spin $S = 1/2$ and $S = 1$ chains, Phys. Rev. B **53**, 8521 (1996).

[35] K. Hijii, A. Kitazawa, and K. Nomura, Phase diagram of $S = 1/2$ two-leg XXZ spin-ladder systems, Phys. Rev. B **72**, 014449 (2005).

[36] Y. Q. Li, M. Ma, D. N. Shi, and F. C. Zhang, SU(4) Theory for Spin Systems with Orbital Degeneracy, Phys. Rev. Lett. **81**, 3527 (1998).

[37] I. Affleck, Exact critical exponents for quantum spin chains, non-linear σ-models at $\theta = \pi$ and the quantum Hall effect, Nucl. Phys. B **265**, 409 (1986).

[38] I. Affleck, Critical behaviour of SU(n) quantum chains and topological non-linear σ-models, Nucl. Phys. B **305**, 582 (1988).

[39] S. K. Pati, R. R. P. Singh, and D. I. Khomskii, Alternating Spin and Orbital Dimerization and Spin-Gap Formation in Coupled Spin-Orbital Systems, Phys. Rev. Lett. **81**, 5406 (1998).

[40] C. Itoi, S. Qin, and I. Affleck, Phase diagram of a one-dimensional spin-orbital model, Phys. Rev. B **61**, 6747 (2000).

[41] K. Hijii and K. Nomura, Phase transition of $S = \frac{1}{2}$ two-leg Heisenberg spin ladder systems with a four-spin interaction, Phys. Rev. B **80**, 014426 (2009).

[42] N. J. Robinson, A. Altland, R. Egger, N. M. Gergs, W. Li, D. Schuricht, A. M. Tsvelik, A. Weichselbaum, and R. M. Konik, Nontopological Majorana Zero Modes in Inhomogeneous Spin Ladders, Phys. Rev. Lett. **122**, 027201 (2019).

[43] A. A. Nersesyan and A. M. Tsvelik, One-Dimensional Spin-Liquid without Magnon Excitations, Phys. Rev. Lett. **78**, 3939 (1997).

[44] M. Müller, T. Vekua, and H.-J. Mikeska, Perturbation theories for the $S = 1/2$ spin ladder with a four-spin ring exchange, Phys. Rev. B **66**, 134423 (2002).

[45] S. Takayoshi and M. Sato, Coefficients of bosonized dimer operators in spin-$\frac{1}{2}$ XXZ chains and their applications, Phys. Rev. B **82**, 214420 (2010).

[46] Y. Wang, Exact solution of a spin-ladder model, Phys. Rev. B **60**, 9236 (1999).

[47] A. Läuchli, G. Schmid, and M. Troyer, Phase diagram of a spin ladder with cyclic four-spin exchange, Phys. Rev. B **67**, 100409(R) (2003).

[48] T. Hikihara, T. Momoi, and X. Hu, Spin-Chirality Duality in a Spin Ladder with Four-Spin Cyclic Exchange, Phys. Rev. Lett. **90**, 087204 (2003).

[49] K. Hijii and K. Nomura, Universality class of an $S = \frac{1}{2}$ quantum spin ladder system with four-spin exchange, Phys. Rev. B **65**, 104413 (2002).

[50] K. Hijii, S. Qin, and K. Nomura, Staggered dimer order and criticality in an $S = \frac{1}{2}$ quantum spin ladder system with four-spin exchange, Phys. Rev. B **68**, 134403 (2003).

[51] S. Brehmer, H.-J. Mikeska, M. Müller, N. Nagaosa, and S. Uchida, Effects of biquadratic exchange on the spectrum of elementary excitations in spin ladders, Phys. Rev. B **60**, 329 (1999).

[52] M. Matsuda, K. Katsumata, R. S. Eccleston, S. Brehmer, and H.-J. Mikeska, Magnetic excitations and exchange interactions in the spin-$\frac{1}{2}$ two-leg ladder compound $La_6Ca_8Cu_{24}O_{41}$, Phys. Rev. B **62**, 8903 (2000).

[53] T. Giamarchi, *Quantum Physics in One Dimension*, International Series of Monographs on Physics (Oxford University Press, New York, 2004).

[54] A. Gogolin, A. Nersesyan, and A. Tsvelik, *Bosonization and Strongly Correlated Systems* (Cambridge University Press, New York, 2004).

[55] S. Lukyanov and A. Zamolodchikov, Exact expectation values of local fields in the quantum sine-gordon model, Nucl. Phys. B **493**, 571 (1997).

[56] T. Hikihara and A. Furusaki, Correlation amplitude for the $S = \frac{1}{2}$ XXZ spin chain in the critical region: Numerical renormalization-group study of an open chain, Phys. Rev. B **58**, R583 (1998).

[57] T. Hikihara, A. Furusaki, and S. Lukyanov, Dimer correlation amplitudes and dimer excitation gap in spin-$\frac{1}{2}$ XXZ and Heisenberg chains, Phys. Rev. B **96**, 134429 (2017).

[58] P. Lecheminant, A. O. Gogolin, and A. A. Nersesyan, Criticality in self-dual sine-Gordon models, Nucl. Phys. B **639**, 502 (2002).

[59] M. Tsuchiizu and A. Furusaki, Generalized two-leg Hubbard ladder at half filling: Phase diagram and quantum criticalities, Phys. Rev. B **66**, 245106 (2002).

[60] P. Calabrese and J. Cardy, Entanglement entropy and quantum field theory, J. Stat. Mech. (2004) P06002.

[61] F. Pollmann, S. Mukerjee, A. M. Turner, and J. E. Moore, Theory of Finite-Entanglement Scaling at One-Dimensional Quantum Critical Points, Phys. Rev. Lett. **102**, 255701 (2009).

[62] C. Wang, A. Nahum, M. A. Metlitski, C. Xu, and T. Senthil, Deconfined Quantum Critical Points: Symmetries and Dualities, Phys. Rev. X **7**, 031051 (2017).

[63] D. F. Mross, J. Alicea, and O. I. Motrunich, Symmetry and Duality in Bosonization of Two-Dimensional Dirac Fermions, Phys. Rev. X **7**, 041016 (2017).

[64] M. M. Rams, P. Czarnik, and L. Cincio, Precise Extrapolation of the Correlation Function Asymptotics in Uniform Tensor Network States with Application to the Bose-Hubbard and XXZ Models, Phys. Rev. X **8**, 041033 (2018).

[65] We indeed found that our data at the Néel-SD transition point followed this power-law scaling but with $\kappa \simeq 1.2$ instead of $\kappa = 6/(\sqrt{12}+1) \simeq 1.344$ for $c = 1$. The disagreement in κ is possibly due to the interplay between the symmetric and antisymmetric channels for a finite bond dimension χ.

[66] This error estimation is expected to be sufficient for the following reason. We performed extrapolation assuming the linear scaling of $\xi(\chi)$ with $1/\chi$ for the transverse-field Ising chain, and the extrapolated correlation length $\xi(\chi \to \infty)$ was off the exact solution at worst 5%. This indicates that if we had two decoupled copies of the transverse-field Ising chains and described them using a single uniform MPS, extrapolation based on the linear scaling of $\xi(\chi)$ with $1/\sqrt{\chi}$ would result in the same error.